Materials Research. 2021; 24(2): e20200232
DOI: https://doi.org/10.1590/1980-5373-MR-2020-0232

Fabrication of New Fe_3O_4/PVA/$(C_6H_7O_6Na)_n$ Nanohybrid Ferrogels for Antibacterial Applications

Ahmad Taufiq[a*], *Anggra D. Iswatin*[a], *Rosy E. Saputro*[a], *Chusnana I. Yogihati*[a], *Nurul Hidayat*[a], *Markus Diantoro*[a], *Sunaryono*[a], *Munasir*[b]

[a]*Universitas Negeri Malang, Faculty of Mathematics and Natural Sciences, Department of Physics, 65145, Malang, Indonesia.*

[b]*Universitas Negeri Surabaya, Faculty of Mathematics and Natural Sciences, Department of Physics, Kampus UNESA Ketintang, 60231, Surabaya, Indonesia.*

Received: May 29, 2020; Revised: October 17, 2020; Accepted: December 27, 2020

New Fe_3O_4/polyvinyl alcohol (PVA)/sodium alginate $(C_6H_7O_6Na)_n$ nanohybrid ferrogels for antibacterial applications were fabricated. The crystal and molecular structures along with optical and magnetic properties of the prepared samples were characterized. The antibacterial activity of the ferrogels against *Bacillus subtilis* and *Escherichia coli* was investigated using the agar dilution method. X-ray diffraction analysis showed that the Fe_3O_4/PVA comprised a PVA amorphous phase and a spinel-structured Fe_3O_4 crystalline phase. The Fe_3O_4/PVA crystallite size was 7.5–9.9 nm and the scanning electron micrographs showed that the Fe_3O_4/PVA agglomerated. The ferrogels were superparamagnetic with saturation magnetizations from 14.8×10^{-3} to 82.1×10^{-3} emu/g. The absorption of the ferrogels showed a bathochromic effect, accompanied by an increase in the bandgap from 2.09 to 2.18 eV with increasing Fe_3O_4 content in the ferrogels. The ferrogels demonstrated new potency as antibacterial agents against *B. subtilis* and *E. coli*, where their antibacterial performance increased with increasing Fe_3O_4 content.

Keywords: *Fe_3O_4/PVA/$(C_6H_7O_6Na)_n$, nanohybrid, ferrogels, superparamagnetic, antibacterial agent.*

1. Introduction

Over the past few decades, researchers have widely developed methods of preparing Fe_3O_4 nanoparticles (NPs) in various shapes and sizes and in the forms of powders, films, ferrofluids, and ferrogels. In particular, intensive research on Fe_3O_4 NPs in the form of ferrogels has been motivated by their advantageous properties compared with those of other forms, even ferrofluids. Theoretically, Fe_3O_4 ferrogels, which are gels with a cross-linked polymer network containing Fe_3O_4 NPs as a filler, offer specific advantages over conventional gels with respect to their high flexibility and high sensitivity to an external magnetic field, which implies that ferrogels can be easily positioned inside a living organism[1].

Fe_3O_4 NPs exhibit superior advantageous properties, including superparamagnetism, biocompatibility, and low toxicity. They are also inexpensive and easily synthesized[2], making such materials attractive in the biomedical field[3], for example, as antibacterial agents for skin infections. In general, skin infections occur and often pose therapeutic challenges because of increasing concerns about multidrug-resistant bacteria[4]. Furthermore, gel-based skin antibacterial agents are particularly attractive because gels have advantages over powders and liquids. However, the Fe_3O_4-based antibacterial agents developed thus far have been based on powders. Therefore, the development of Fe_3O_4 ferrogels as antibacterial agents is strongly desired.

Fe_3O_4 ferrogels based on polyvinyl alcohol (PVA) have recently begun to attract researchers' attention for possible use in various multipurpose applications[5–7]. Recent research has shown that Fe_3O_4 ferrogels with a PVA matrix have excellent prospects for use in biomedical applications[8]. However, for skin antibacterial applications, PVA has a drawback because of its relatively high stiffness, which reduces antibacterial efficacy. Consequently, an appropriate biocompatible crosslinking agent that reduces the stiffness of Fe_3O_4/PVA ferrogels is urgently needed.

Sodium alginate, with chemical formula $(C_6H_7O_6Na)_n$, exhibits strong potential for use as a crosslinking agent that supports the antimicrobial performance of Fe_3O_4/PVA ferrogels. Theoretically, in addition to reducing the stiffness of PVA[9], $(C_6H_7O_6Na)_n$ offers other advantages of nontoxicity, biocompatibility[10], bioresorption ability, biodegradability, good mechanical properties, and relatively low cost[11,12]. Therefore, in the present work, we developed new Fe_3O_4/PVA/$(C_6H_7O_6Na)_n$ nanohybrid ferrogels as antibacterial agents and investigated their crystal and molecular structures, optical properties, bandgaps, magnetic behaviors, and antibacterial efficacy.

*e-mail: ahmad.taufiq.fmipa@um.ac.id

2. Experimental Methods

2.1 Materials

The main precursors were $FeCl_2 \cdot 6H_2O$, $FeCl_3 \cdot 6H_2O$, HCl (12 M), NH_4OH (6.5 M), PVA ($M_w \approx 60{,}000$), and $(C_6H_7O_6Na)_n$. All precursors were analytical grade to ensure high purity and quality of the samples. All precursors were purchased from Merck and were used without further purification.

2.2 Fabrication of Fe_3O_4/PVA Nanocomposites

The Fe_3O_4 NPs were prepared using a coprecipitation method following the procedure described in our previous work[13]. One g of PVA was dissolved in 20 mL of distilled water at 120 °C for 3 h using a magnetic stirrer with a speed of 720 rpm. Various masses of Fe_3O_4 (0.13, 0.26, 0.39, 0.52, and 0.65 g) were mixed with 2 mL of PVA solution at 120 °C for 30 min using a magnetic stirrer with a speed of 720 rpm to produce Fe_3O_4/PVA. The Fe_3O_4/PVA was collected after the mixture cooled to room temperature. The samples were labeled S1–S5 according to the respective masses of Fe_3O_4 (0.13, 0.26, 0.39, 0.52, and 0.65 g).

2.3 Fabrication of Fe_3O_4/PVA/$(C_6H_7O_6Na)_n$ Ferrogels

The Fe_3O_4/PVA/$(C_6H_7O_6Na)_n$ nanohybrid ferrogels were prepared through a sonochemical method. Three hundred mg of $(C_6H_7O_6Na)_n$ was dissolved in 20 mL of distilled water at 120 °C under stirring using a magnetic stirrer with a speed of 720 rpm for 4 h, followed by a cooling process to room temperature. Next, 2 mL of $(C_6H_7O_6Na)_n$ solution was reacted with the prepared Fe_3O_4/PVA (S1–S5 samples) at 120 °C for 30 min under stirring using a magnetic stirrer with a speed of 720 rpm. After the mixtures cooled to room temperature, the final products were obtained as solid-black gels in the form of Fe_3O_4/PVA/$(C_6H_7O_6Na)_n$ nanohybrid ferrogels. The prepared Fe_3O_4/PVA/$(C_6H_7O_6Na)_n$ nanohybrid ferrogels were labeled SF1–SF5 according to the respective S1–S5 samples. The schematic showing the construction of the Fe_3O_4/PVA/$(C_6H_7O_6Na)_n$ nanohybrid ferrogels is shown in Figure 1.

2.4 Characterization

The structural, optical, and magnetic properties were characterized by X-ray diffraction (XRD) for S1–S5 samples, scanning electron microscopy/energy-dispersive X-ray spectroscopy (SEM/EDX) for S1–S5 samples, UV–Vis spectrophotometry for SF1–SF5 samples, Fourier transform infrared (FTIR) spectroscopy for SF1–SF5 samples, and vibrating sample magnetometry for SF1–SF5 samples. The antimicrobial performance of the SF1–SF5 samples against *Bacillus subtilis* (Gram-positive) and *Escherichia coli* (Gram-negative) was evaluated through the agar diffusion method. All characterizations were conducted at ambient temperature.

3. Results and Discussion

The XRD patterns of the Fe_3O_4/PVA used as the filler of the ferrogels (Figure 2) show that two phases were formed, i.e., amorphous and crystalline phases. The amorphous phase, with a broad diffraction peak detected at 2θ of approximately 19.5°, was attributed to PVA. This is consistent with the results of the previous work[14]. Meanwhile, the XRD patterns of the crystalline phase showed diffraction peaks at 2θ of 30.1°, 35.6°, 43.3°, 57.3°, and 63.0°, which represent the (200), (311), (400), (422), (511), and (440) planes of Fe_3O_4, respectively[15]. Furthermore, the intensities of the Fe_3O_4 peaks were observed to increase with increasing Fe_3O_4 content. Interestingly, the increase in Fe_3O_4 content led to a decrease in the intensity of the peak of the PVA amorphous phase because of the reduced PVA content. The crystallinity, i.e., the degree of regularity and structural order in the Fe_3O_4/PVA

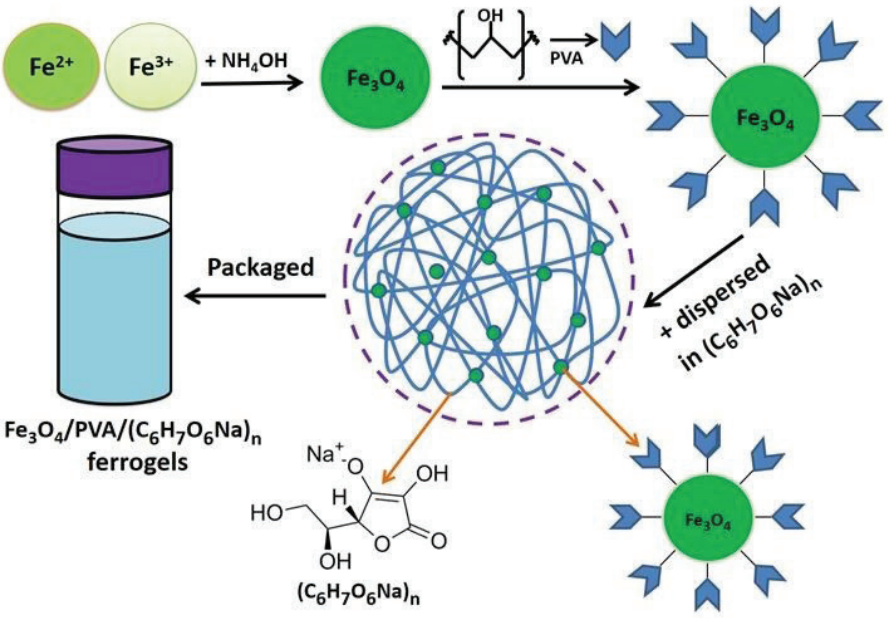

Figure 1. Schematic showing the construction of the Fe_3O_4/PVA/$(C_6H_7O_6Na)_n$ nanohybrid ferrogels.

system, was found to increase from 22.8% to 61.0% with increasing Fe_3O_4 content.

The Fe_3O_4 crystal structure in this study exhibited a cubic spinel structure. The lattice parameters of the Fe_3O_4 in all samples were constant, with a value of $a = b = c = 8.365$ Å.

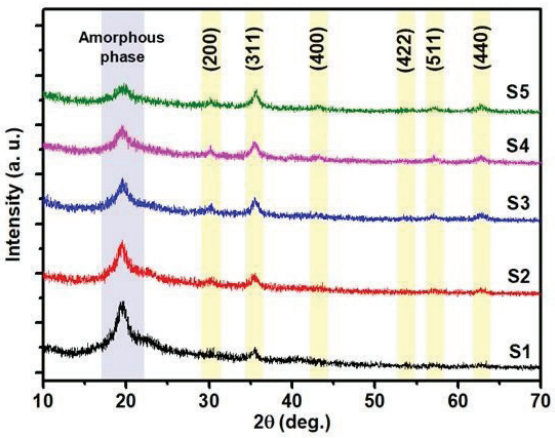

Figure 2. XRD patterns of the Fe_3O_4/PVA.

In this crystal structure, the Fe^{2+} and Fe^{3+} ions are distributed in octahedral and tetrahedral sites. The distribution of these metallic ions determines the magnetic moments of Fe_3O_4, where the magnetic moments between ions in octahedral and tetrahedral sites are anti-parallel. Furthermore, the crystallite size (D) of the Fe_3O_4 of all samples was calculated using the Debye–Scherrer equation: $D = 0.9\lambda/\beta\cos\theta$, where λ, β, and θ are the wavelength of the X-rays, the full-width at half-maximum of the peak, and the diffraction angle, respectively[16]. The data analysis results in Table 1 show that D increased with increasing Fe_3O_4 content. The increasing Fe_3O_4 content tended to increase the extent of aggregation into clusters because of the concomitant increase in the

Table 1. Crystallite parameters of the Fe_3O_4/PVA

Sample	$a = b = c$ (Å)	Crystallite size (nm)	Crystallinity (%)
S1	8.365	7.5	22.8
S2	8.365	8.0	30.6
S3	8.365	8.9	46.2
S4	8.365	9.4	53.4
S5	8.365	9.9	61.0

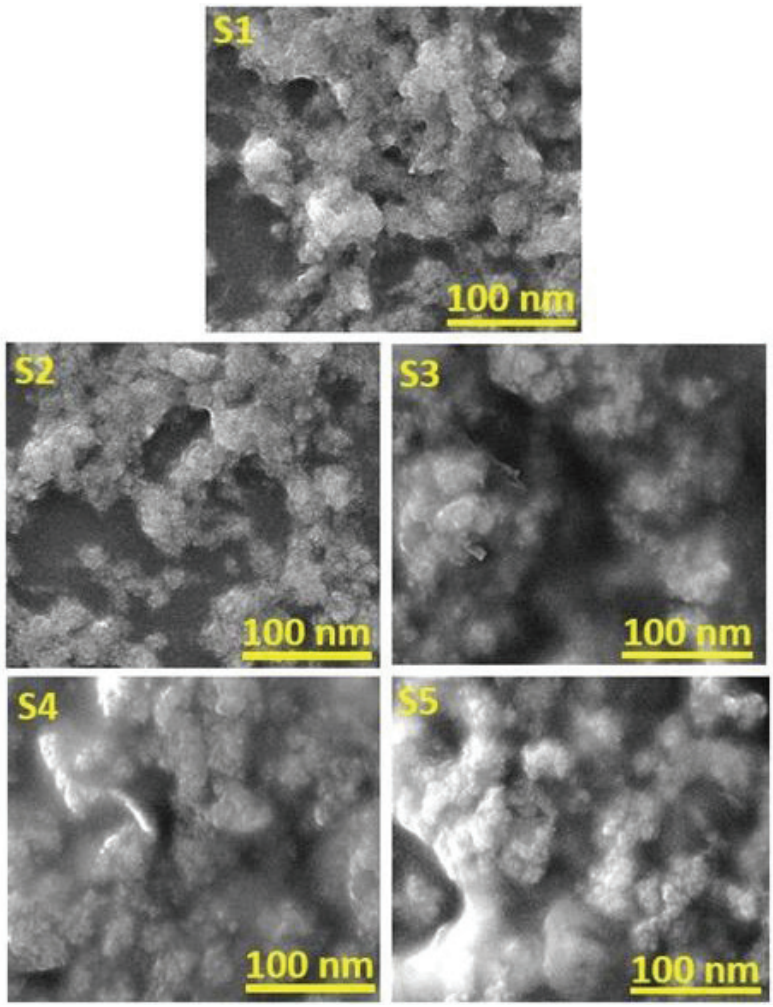

Figure 3. SEM images of the Fe_3O_4/PVA.

van der Waals force. This result is consistent with the SEM images, as shown in Figure 3. The SEM images show that the Fe_3O_4 was covered with PVA, which led to aggregation[17]. As the Fe_3O_4 content was increased, the Fe_3O_4/PVA tended to form more clusters because of the reduced PVA content. Therefore, the Fe_3O_4 NPs, which have a high specific-surface-area-to-volume ratio, tended to agglomerate because of the interaction of magnetic particles or because of van der Waals force. In this regard, Roohani et al. showed that aggregation occurs as a result of hydrogen bonds between particles because PVA, which is rich in hydroxyl groups, cannot cover all of the hydrogen bonding sites of the Fe_3O_4 NPs[18]. The elemental composition of the samples is presented in Table 2. The elemental analysis results indicate that the Fe content increases and the C content decreases with increasing Fe_3O_4 used in the synthesis.

The transmittance spectra used to characterize the functional groups of the Fe_3O_4/PVA/$(C_6H_7O_6Na)_n$ ferrogels are presented in Figure 4. The Fe–O stretching band originating from Fe_3O_4 is observed at 420–500 cm^{-1} for the tetragonal sites and at 700 cm^{-1} for the octahedral sites. Furthermore, stretching bands characteristic of PVA were detected at 857 cm^{-1} (CC stretching)[19], 1047–1147 cm^{-1} (C–O)[20], 1350 cm^{-1} (=C–O–C), and 2966 cm^{-1} (CH_2 asymmetric stretching)[21]. The stretching bands characteristic of $(C_6H_7O_6Na)_n$ were detected in the range 1473–1560 cm^{-1} (COO symmetric and asymmetric)[22] and at 1708 cm^{-1} (C=O)[23]. Interestingly, the Fe_3O_4, PVA, and $(C_6H_7O_6Na)_n$, as the main components of the ferrogels, all contributed to the broad O–H band between 3305 and 3670 cm^{-1}.

The contribution of Fe_3O_4, PVA, and $(C_6H_7O_6Na)_n$ to the functional bonding observed by the FTIR spectra initiates further discussion. The changes in intensities of chemical bands provide a clue on the mechanical reorientation of the molecules[24]. The decreasing intensities of O-H band, CH_2 asymmetric stretching, =C–O–C, and C–O bonding is believed due to the decrease of PVA content. This trend is related to the increase of Fe_3O_4 and the presence of alginate. From the theoretical viewpoint, the presence of alginate reduces the stiffness of PVA-based system by virtue of its low elongation break[25]. In other words, the long-chain structure of PVA in Fe_3O_4/PVA nanocomposites was destroyed by the addition of alginate. Zhang et al. claimed that one of the best ways to reduce the stiffness of fabric-reinforced PVA was by introducing Na-alginate[26]. They discovered that mechanical strength and stiffness could be decreased due to the swelling behavior of composite hydrogels that diminish friction amongst interfibers[26]. Furthermore, alginate is not only effective in reducing the stiffness of PVA-fibers, but also other polymers, such as poly-lactic-co-glycolic acid[27].

The absorbance spectra, as shown in Figure 5, were recorded to investigate the optical properties of the Fe_3O_4/PVA/$(C_6H_7O_6Na)_n$ ferrogels. The peaks at 474 and 511 nm are consistent with the previous work[28]. The absorbance intensity is associated with the number of particles present. Meanwhile, the wavelength of maximum absorption is associated with the particle size. Physically, these peaks represent the difference in energy levels between the σ and π* states[29]. In addition, incorporating the Fe_3O_4 into ferrogels would increase the distribution of particles embedded in the $(C_6H_7O_6Na)_n$ crosslinking agent. As a consequence, the conduction electrons on the surface of the Fe_3O_4 migrate from one atom to neighboring atoms so that the surface plasmon resonance shifts toward lower energies, which is associated with smaller wavelengths[30]. In physics, this phenomenon is described as the bathochromic effect. The bandgap (E_g) of the Fe_3O_4/PVA/$(C_6H_7O_6Na)_n$ was calculated using the equation $\alpha h\upsilon = A(h\upsilon - E_g)^{1/2}$, where α, h, υ, and A are the absorption coefficient, Planck's constant, the frequency, and a constant, respectively[31]. The linear part of the curve was extrapolated to the intersection with the energy axis to determine the bandgap[32]. The data analysis is shown in Figure 6. The E_g of the Fe_3O_4/PVA/$(C_6H_7O_6Na)_n$ ferrogels

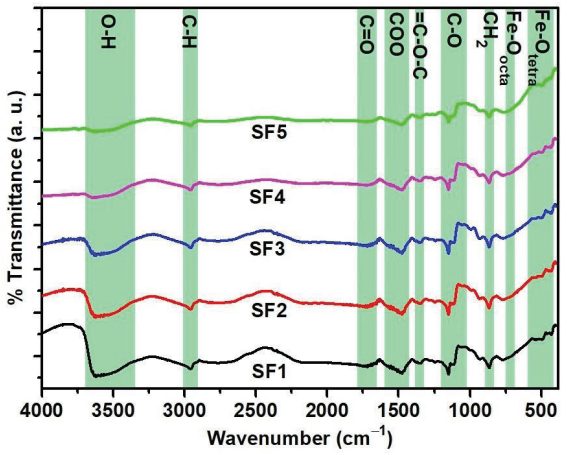

Figure 4. FTIR spectra of the Fe_3O_4/PVA/$(C_6H_7O_6Na)_n$ ferrogels.

Table 2. Elemental composition of the Fe_3O_4/PVA

Sample	Wt. (%)		
	Fe	O	C
S1	9.6	35.7	54.7
S2	12.9	37.1	50.0
S3	22.7	35.3	42.0
S4	29.9	30.5	39.6
S5	34.2	30.9	34.9

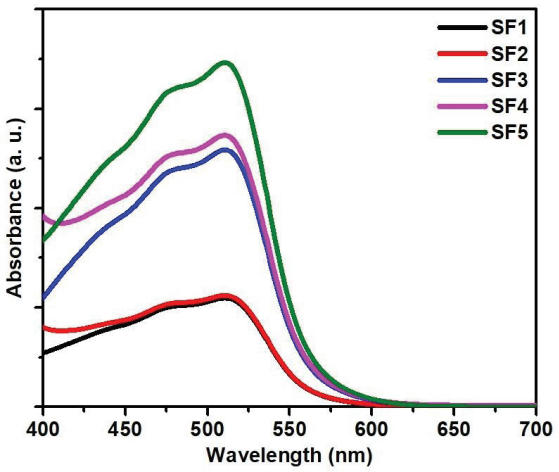

Figure 5. Absorbance spectra of the Fe_3O_4/PVA/$(C_6H_7O_6Na)_n$ ferrogels.

increased from 2.09 eV to 2.18 eV with increasing Fe_3O_4 content. This phenomenon is explained by Fe_3O_4 reduced dissociation as a result of its increased dispersion in the ferrogels. It implies that collisions among electrons in the magnetic particles were reduced, resulting in an increase of the energy on the surface. Other authors have reported an E_g of slightly greater than 2.2 eV for Fe_3O_4[33]. This difference is attributed to the effect of the surface modification of Fe_3O_4 using PVA, which led to dispersion of the Fe_3O_4 in $(C_6H_7O_6Na)_n$ to form nanohybrid ferrogels.

The magnetization curves of the Fe_3O_4/PVA/$(C_6H_7O_6Na)_n$ ferrogels are depicted in Figure 7. The figure shows that all of the samples are likely to exhibit superparamagnetic character, as indicated by the characteristic S-like shape with the coercivity field close to zero[34]. A quantitative analysis was carried out to fit the magnetization curves using the Langevin equation:

$$M = M_s\left(\coth\left(\frac{\mu H}{k_B T}\right) - \left(\frac{k_B T}{\mu H}\right)\right) \quad (1)$$

where M, M_s, μ, H, k_B, and T are the magnetization, saturation magnetization, magnetic moment, Boltzmann constant, and temperature, respectively. The magnetic parameters obtained from the data analysis are presented in Table 3. The magnetic moment of the Fe_3O_4/PVA/$(C_6H_7O_6Na)_n$ ferrogels increased by the addition of Fe_3O_4 content. The magnetic moment plays an essential role in a material's response to an external magnetic field. Interestingly, not only the increase in Fe_3O_4 content but also the increase in particle size contributed to

Table 3. Magnetic parameters of the Fe_3O_4/PVA/$(C_6H_7O_6Na)_n$ ferrogels

Sample	M_s ($\times 10^{-3}$ emu/g)	H_c (T)	Magnetic moment ($\times 10^{-19}$ J/T)
SF1	14.8	0.013	8.1
SF2	16.8	0.016	8.7
SF3	42.1	0.020	9.5
SF4	64.3	0.025	10.1
SF5	82.1	0.028	14.0

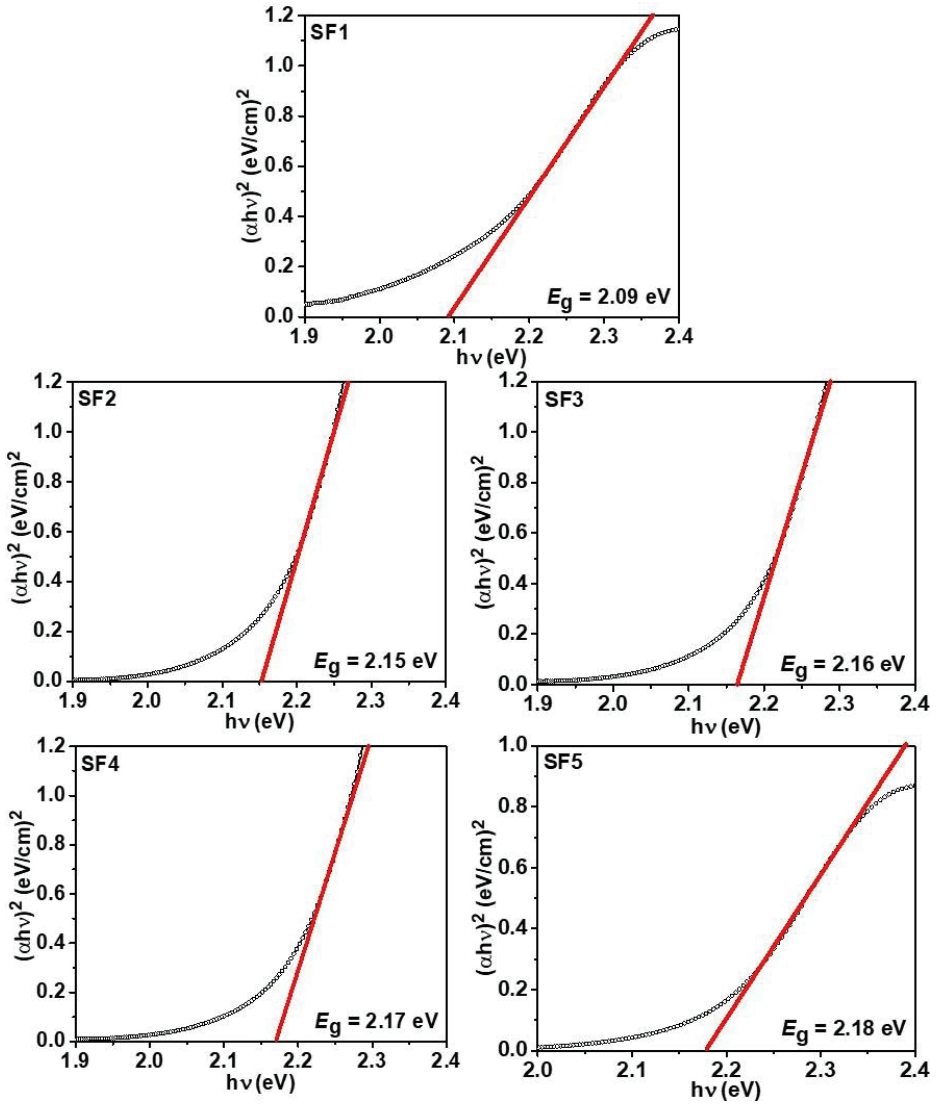

Figure 6. Bandgaps of the Fe_3O_4/PVA/$(C_6H_7O_6Na)_n$ ferrogels.

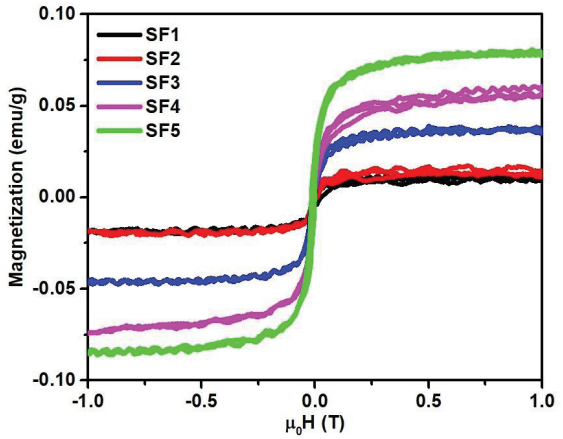

Figure 7. Magnetization curves of the Fe_3O_4/PVA/$(C_6H_7O_6Na)_n$ ferrogels.

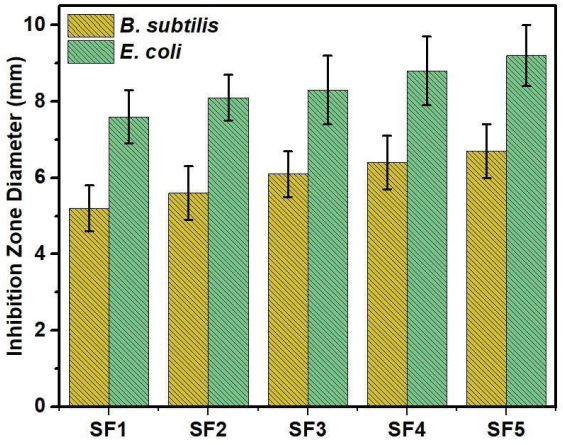

Figure 8. Inhibition-zone diameter of the Fe_3O_4/PVA/$(C_6H_7O_6Na)_n$ ferrogels.

the increase in M_s. Karaagac et al. have similarly reported that particle size strongly influences the M_s[35]. Furthermore, the coercivity field also increased with increasing Fe_3O_4 content, which is attributable to the accompanying increase in particle size. Previous work has shown the same trend for Fe_3O_4/PVA with a ribbon-like structure[36].

The antibacterial performance of the Fe_3O_4/PVA/$(C_6H_7O_6Na)_n$ ferrogels against *B. subtilis* and *E. coli* is presented in Figure 8. This figure shows that the inhibition-zone diameter increases with increasing Fe_3O_4 content. The inhibition-zone is associated with the antibacterial performance of the Fe_3O_4/PVA/$(C_6H_7O_6Na)_n$ ferrogels. Theoretically, the ability to destroy bacteria is strongly correlated with the ability of the Fe_3O_4/PVA/$(C_6H_7O_6Na)_n$ to generate reactive oxygen species (ROS)[37]. ROS generate superoxide as a free radical that inhibits bacterial growth[38]. Furthermore, in the case of Fe_3O_4 NPs incorporated into ferrogels, the inhibition-zone diameter was larger than that of pure Fe_3O_4. The enhanced bactericidal activity of the Fe_3O_4/PVA/$(C_6H_7O_6Na)_n$ ferrogels is attributed to the better dispersion of the Fe_3O_4 particles in the ferrogels than in the pure Fe_3O_4, which tends to aggregate. In addition to ROS, particle size also plays an important role in bactericidal activity. Other authors have shown that Fe_3O_4 with small particle size and monodisperse shape exhibits better inhibitory activity against bacteria than Fe_3O_4 with large particle size and polydisperse shape[39]. Theoretically, Fe_3O_4 NPs with an excellent particle size distribution are likely to penetrate more easily into the walls or pores of bacteria. As a comparison, Jalali et al. prepared Fe_3O_4 NPs by doping Co and Zn to strengthen their antibacterial potential; however, they observed an inhibition-zone diameter of only 6.4 mm for *E. coli*[40]. In line with that, Salem and co-workers fabricated Fe_3O_4 NPs from marine algae; however, the inhibition zone diameter for *E. coli* was still approximately 6 mm and that for *B. subtilis* was approximately 5 mm. These values are still inferior compared with that of the ferrogels investigated in the present study.

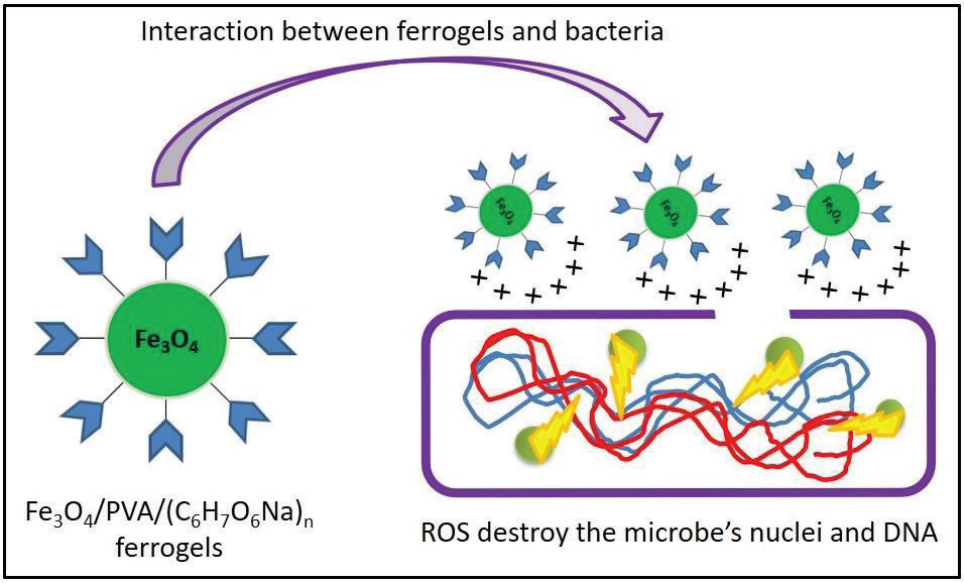

Figure 9. Bactericidal mechanism of the Fe_3O_4/PVA/$(C_6H_7O_6Na)_n$ ferrogels.

The bactericidal mechanism of the Fe_3O_4/PVA/$(C_6H_7O_6Na)_n$ ferrogels is presented in Figure 9. From a physics perspective, the negative surface charges on the Fe_3O_4/PVA nanocomposite particles repel the bacteria under electrostatic interaction mechanism. This repulsion makes the metal oxide NPs less effective in destroying bacteria. However, when Fe_3O_4/PVA are dispersed in $(C_6H_7O_6Na)_n$, the net charge at the surface of the particles becomes positive. This change in surface charge is beneficial in terms of catching the bacteria by Fe_3O_4/PVA/$(C_6H_7O_6Na)_n$ ferrogels. Thus, the chance of ROS penetrating into the bacteria increases. This leads to increase in the diameter of the inhibition zone. Thus, the Fe_3O_4/PVA/$(C_6H_7O_6Na)_n$ nanohybrid ferrogels exhibit superior antibacterial activity. Furthermore, because of the structural complexity of the Fe_3O_4 ferrogels, a theoretical explanation of the performance of the ferrogels related to their magnetic-sensitive behavior has not yet been established. Therefore, for the Fe_3O_4/PVA/$(C_6H_7O_6Na)_n$ ferrogels to be used on a large scale, further investigation is necessary, especially with respect to the optimum filler, matrix, cross-linker contents in the ferrogels.

4. Conclusion

We synthesized new Fe_3O_4/PVA/$(C_6H_7O_6Na)_n$ nanohybrid ferrogels using a combination of coprecipitation and sonochemical methods. The XRD data indicated the presence of two phases: amorphous PVA and crystalline Fe_3O_4. The crystallite size and crystallinity increased with the addition of Fe_3O_4. The surface of the Fe_3O_4/PVA/$(C_6H_7O_6Na)_n$ agglomerated because of the increase in Fe_3O_4 content, preventing PVA from covering it optimally. The nanohybrid ferrogels exhibited superparamagnetism, where the coercivity field and magnetization saturation increased with increasing Fe_3O_4 content. Remarkably, the antibacterial activity of the ferrogels was observed to increase with increasing Fe_3O_4 content, which was attributed to an increase in ROS penetrating the bacteria.

5. Acknowledgments

This work was financially supported by KEMENRISTEKDIKTI 2019 for AT.

6. References

1. Blyakhman F, Makarova EB, Fadeyev FA, Lugovets DV, Safronov AP, Shabadrov PA, et al. The contribution of magnetic nanoparticles to ferrogel biophysical properties. Nanomaterials (Basel). 2019;9(2):232. http://dx.doi.org/10.3390/nano9020232. PMid:30744036.
2. Taufiq A, Nikmah A, Hidayat A, Sunaryono S, Mufti N, Hidayat N, et al. Synthesis of magnetite/silica nanocomposites from natural sand to create a drug delivery vehicle. Heliyon. 2020;6(4):e03784. http://dx.doi.org/10.1016/j.heliyon.2020.e03784. PMid:32322741.
3. Karimzadeh I, Aghazadeh M, Dalvand A, Doroudi T, Kolivand PH, Ganjali MR, et al. Effective electrosynthesis and in situ surface coating of Fe_3O_4 nanoparticles with polyvinyl alcohol for biomedical applications. Mater Res Innov. 2019;23:1-8.
4. Chen MX, Alexander KS, Baki G. Formulation and evaluation of antibacterial creams and gels containing metal ions for topical application. J Pharm (Cairo). 2016;2016:1-10. http://dx.doi.org/10.1155/2016/5754349. PMid:27885352.
5. Soleymani M, Akbari A, Mahdavinia GR. Magnetic PVA/lLponite RD hydrogel nanocomposites for adsorption of model protein BSA. Polym Bull. 2019;76(5):2321-40. http://dx.doi.org/10.1007/s00289-018-2480-1.
6. Sunaryono, Hidayat MF, Kholifah MN, Hidayat S, Mufti N, Taufiq A. Magneto-thermal behavior of $Mn_xFe_{3-x}O_4$-PVA/PVP magnetic hydrogel and its potential application. AIP Conf Proc. 2020;2228:030018. http://dx.doi.org/10.1063/5.0000890.
7. Sunaryono, Hidayat MF, Yogihati CI, Taufiq A, Mufti N, Rahmawati R. Concentration effect of ferrofluids in ferrogels on their magnetic and magneto-elasticity behaviors. Materials Today: Proceedings. 2019;17:1720-7.
8. Wang Y, Zhu Y, Xue Y, Wang J, Li X, Wu X, et al. Sequential in-situ route to synthesize novel composite hydrogels with excellent mechanical, conductive, and magnetic responsive properties. Mater Des. 2020;193:108759. http://dx.doi.org/10.1016/j.matdes.2020.108759.
9. Rafienia M, Saberi A, Poorazizi E. A Novel Fabrication of PVA/alginate-bioglass electrospun for biomedical engineering application. Nanomedicine Journal. 2017;4:152-63.
10. Yeung RA, Kennedy RA. A comparison of selected physico-chemical properties of calcium alginate fibers produced using two different types of sodium alginate. J Mech Behav Biomed Mater. 2019;90:155-64. http://dx.doi.org/10.1016/j.jmbbm.2018.10.011. PMid:30366306.
11. Furuya DC, Costa SA, Oliveira RC, Ferraz HG, Pessoa Junior A, Costa SM. Fibers obtained from alginate, chitosan and hybrid used in the development of scaffolds. Mater Res. 2017;20(2):377-86. http://dx.doi.org/10.1590/1980-5373-mr-2016-0509.
12. Kurowiak J, Kaczmarek-Pawelska A, Mackiewicz AG, Bedzinski R. Analysis of the degradation process of alginate-based hydrogels in artificial urine for use as a bioresorbable material in the treatment of urethral injuries. Processes (Basel). 2020;8(3):304. http://dx.doi.org/10.3390/pr8030304.
13. Eko Saputro R, Taufiq A, Hidayat N, Sunaryono, Amalia Hariyanto Y, Hidayat A. Preparation of Fe_3O_4/OA/DMSO ferrofluids using a double surfactant system as antifungal materials candidate. IOP Conf Series Mater Sci Eng. 2019;515:012029. http://dx.doi.org/10.1088/1757-899X/515/1/012029.
14. Wang P, Zhang M, Liu Y, Wang L, Lv Q, Xu D, et al. One-step synthesis of hydrophilic graphene-Fe_3O_4-PVA composite film: micromorphology and performance. J Appl Polym Sci. 2019;136(44):48174. http://dx.doi.org/10.1002/app.48174.
15. Taufiq A, Ikasari FN, Hidayat N, Ulya HN, Saputro RE, Mufti N, et al. Dependence of PEO content in the preparation of Fe_3O_4/PEO/TMAH ferrofluids and their antibacterial activity. J Polym Res. 2017;27(5):117. http://dx.doi.org/10.1007/s10965-020-02100-w.
16. Ebadi M, Zolfaghari MR, Aghaei SS, Zargar M, Shafiei M, Zahiri HS, et al. A bio-inspired strategy for the synthesis of zinc oxide nanoparticles (Zno Nps) using the cell extract of cyanobacterium Nostoc sp. EA03: from biological function to toxicity evaluation. RSC Advances. 2019;9(41):23508-25. http://dx.doi.org/10.1039/C9RA03962G.
17. Sanaeifar N, Rabiee M, Abdolrahim M, Tahriri M, Vashaee D, Tayebi L. a novel electrochemical biosensor based on fe_3o_4 nanoparticles-polyvinyl alcohol composite for sensitive detection of glucose. Anal Biochem. 2017;519:19-26. http://dx.doi.org/10.1016/j.ab.2016.12.006. PMid:27956150.
18. Roohani M, Shabanian M, Kord B, Hajibeygi M, Khonakdar HA. New functional Fe_3O_4 nanoparticles utilizing as adjuvant in the green PVA/cellulose whiskers nanocomposite. Thermochim Acta. 2016;635:17-25. http://dx.doi.org/10.1016/j.tca.2016.04.020.
19. Zidan HM, Abdelrazek EM, Abdelghany AM, Tarabiah AE. Characterization and some physical studies of PVA/PVP filled

with MWCNTs. Journal of Materials Research and Technology. 2019;8(1):904-91. http://dx.doi.org/10.1016/j.jmrt.2018.04.023.

20. Han Z, Jin J, Wang Y, Zhang Z, Gu J, Ou M, et al. Encapsulating TiO_2 into polyvinyl alcohol coated polyacrylonitrile composite beads for the effective removal of methylene blue. J Braz Chem Soc. 2019;30:211-23.
21. Siddaiah T, Ojha P, Kumar NOGVR, Ramu C. Structural, optical and thermal characterizations of PVA/MAA:EA polyblend films. Mater Res. 2018;21(5):e20170987. http://dx.doi.org/10.1590/1980-5373-mr-2017-0987.
22. Kurayama F, Mohammed Bahadur N, Furusawa T, Sato M, Suzuki N. Facile preparation of aminosilane-alginate hybrid beads for enzyme immobilization: kinetics and equilibrium studies. Int J Biol Macromol. 2020;150:1203-12. http://dx.doi.org/10.1016/j.ijbiomac.2019.10.130. PMid:31751729.
23. Du Y, Li L, Peng H, Zheng H, Cao S, Lv G, et al. A spray-filming self-healing hydrogel fabricated from modified sodium alginate and gelatin as a bacterial Barrier. Macromol Biosci. 2020;20(2):1900303. http://dx.doi.org/10.1002/mabi.201900303. PMid:31867845.
24. Agudelo-Cuartas C, Granda-Restrepo D, Sobral PJA, Castro W. Determination of mechanical properties of whey protein films during accelerated aging: application of FTIR profiles and chemometric tools. Journal of Food Process Engineering. 2020;e13477.
25. Wang Q, Liu J, Zhang L, Ci M, Zhang X, Jiang Z, et al. Preparation and characterization of polyvinyl alcohol/sodium alginate/pyrovatex Cp composite fibers. Ferroelectrics. 2020;562(1):125-125. http://dx.doi.org/10.1080/00150193.2020.1760600.
26. Zhang R, Wu Y, Lin P, Jia Z, Zhang T, Liu F, et al. Extremely tough hydrogels with cotton fibers reinforced. Adv Eng Mater. 2020;22(11):2000508.
27. Liu X, Nielsen LH, Kłodzińska SN, Nielsen HM, Qu H, Christensen LP, et al. Ciprofloxacin-loaded sodium alginate/poly (Lactic-Co-Glycolic Acid) electrospun fibrous mats for wound healing. Eur J Pharm Biopharm. 2018;123:42-9. http://dx.doi.org/10.1016/j.ejpb.2017.11.004. PMid:29129734.
28. Ghaseminezhad SM, Shojaosadati SA. Data on the role of starch and ammonia in green synthesis of silver and iron oxide nanoparticles. Data Brief. 2016;7:999-1003. http://dx.doi.org/10.1016/j.dib.2016.03.068. PMid:27408911.
29. Liu R, Zhu A. Synthesis, characterization, interfacial interactions, and properties of reduced graphene oxide/Fe_3O_4/polyaniline nanocomposites. Polym Compos. 2019;40(S2):1111-9. http://dx.doi.org/10.1002/pc.24893.
30. Al-Abdallat Y, Jum'h I, Al Bsoul A, Jumah R, Telfah A. Photocatalytic degradation dynamics of methyl orange using coprecipitation synthesized Fe_3O_4 nanoparticles. Water Air Soil Pollut. 2019;230(12):277. http://dx.doi.org/10.1007/s11270-019-4310-y.
31. Bhat P, Naveen Kumar S. K., Nagaraju P. Synthesis and characterization of ZnO-MWCNT nanocomposites for 1-Butanol sensing application at room temperature. Physica B. 2019;570:139-47. http://dx.doi.org/10.1016/j.physb.2019.06.008.
32. Somraksa W, Suwanboon S, Amornpitoksuk P, Randorn C. Physical and photocatalytic properties of CeO_2/ZnO/$ZnAl_2O_4$ ternary nanocomposite prepared by Co-precipitation method. Mater Res. 2020;23(1):e20190627. http://dx.doi.org/10.1590/1980-5373-mr-2019-0627.
33. Kumar M, Sharma A, Maurya IK, Thakur A, Kumar S. Synthesis of ultra small iron oxide and doped iron oxide nanostructures and their antimicrobial activities. Journal of Taibah University for Science. 2019;13(1):280-5. http://dx.doi.org/10.1080/16583655.2019.1565437.
34. Aghazadeh M, Karimzadeh I, Ganjali MR, Mohebi Morad M. A novel preparation method for surface coated superparamagnetic Fe_3O_4 Nanoparticles with vitamin c and sucrose. Mater Lett. 2017;12017(196):392-5. http://dx.doi.org/10.1016/j.matlet.2017.03.064.
35. Karaagac O, Yildiz BB, Köçkar H. The influence of synthesis parameters on one-step synthesized superparamagnetic cobalt ferrite nanoparticles with high saturation magnetization. J Magn Magn Mater. 2019;473:262-7. http://dx.doi.org/10.1016/j.jmmm.2018.10.063.
36. Ardiyanti H, Suharyadi E, Kato T, Iwata S. Crystal structures and magnetic properties of magnetite (Fe_3O_4)/Polyvinyl Alcohol (PVA) Ribbon. AIP Conf Proc. 2016;1725:020007. http://dx.doi.org/10.1063/1.4945461.
37. Hariani PL, Desnelli D, Fatma F, Putri RI, Salni S. Synthesis and characterization of Fe_3O_4 nanoparticles modified with polyethylene glycol as antibacterial material. The Journal of Pure and Applied Chemistry Research. 2018;7(2):122-8. http://dx.doi.org/10.21776/ub.jpacr.2018.007.02.393.
38. Wang Q, Zhou Q, Zhang Q, Shi R, Ma S, Zhao W, et al. Fabrication of novel superoxide anion biosensor based on 3D interface of mussel-inspired Fe_3O_4-$Mn_3(PO_3)_2$@ Ni Foam. Talanta. 2018;179:145-52. http://dx.doi.org/10.1016/j.talanta.2017.10.054. PMid:29310214.
39. Kadhim WKA, Nayef UM, Jabir MS. Polyethylene glycol-functionalized Magnetic (Fe_3O_4) nanoparticles: a good method for a successful antibacterial therapeutic agent via damage DNA molecule. Surf Rev Lett. 2019;26(10):1950079. http://dx.doi.org/10.1142/S0218625X19500793.
40. Jalali SAH, Allafchian A, Bahramian H, Amiri R. An antibacterial study of a new magnetite silver nanocomposite. J Environ Chem Eng. 2017;5(6):5786-92. http://dx.doi.org/10.1016/j.jece.2017.11.016.